Spectral analysis of the transition to turbulence from a dipole in stratified fluids

PIERRE AUGIER † ‡, JEAN-MARC CHOMAZ AND PAUL BILLANT

LadHyX, CNRS, Ecole Polytechnique, 91128 Palaiseau Cedex, France

(Received 24 December 2011)

We investigate the spectral properties of the turbulence generated during the non-linear evolution of a Lamb-Chaplygin dipole in a stratified fluid for a high Reynolds number $Re = 28000$ and a wide range of horizontal Froude number $F_h \in [0.0225\ 0.135]$ and buoyancy Reynolds number $\mathcal{R} = ReF_h{}^2 \in [14\ 510]$. The numerical simulations use a weak hyperviscosity and so are almost DNS. After the nonlinear development of the zigzag instability, both shear and gravitational instabilities develop and lead to a transition to small scales. A spectral analysis shows that this transition is dominated by two kinds of transfers: first, the shear instability induces a direct non-local transfer toward horizontal wavelength of the order of the buoyancy scale $L_b = U/N$, where U is the characteristic horizontal velocity of the dipole and N the Brunt-Väisälä frequency; Second, the destabilization of the Kelvin-Helmholtz billows and the gravitational instability lead to small-scale weakly stratified turbulence. Horizontal spectrum of kinetic energy exhibits a $\varepsilon_K{}^{2/3}k_h^{-5/3}$ power law (where k_h is the horizontal wavenumber and ε_K is the dissipation rate of kinetic energy) from $k_b = 2\pi/L_b$ to the dissipative scales, with an energy deficit between the integral scale and k_b and an excess around k_b. The vertical spectrum of kinetic energy can be expressed as $E(k_z) = C_N N^2 k_z^{-3} + C\varepsilon_K{}^{2/3}k_z^{-5/3}$ where C_N and C are two constants of order unity and k_z is the vertical wavenumber. It is therefore very steep near the buoyancy scale with a $N^2k_z^{-3}$ shape and approaches the $\varepsilon_K{}^{2/3}k_z^{-5/3}$ spectrum for $k_z > k_o$, k_o being the Ozmidov wavenumber which is the crossover between the two scaling laws. A decomposition of the vertical spectra depending on the horizontal wavenumber value shows that the $N^2k_z^{-3}$ power law is associated to large horizontal scales $|\mathbf{k}_h| < k_b$ and the $\varepsilon_K{}^{2/3}k_z^{-5/3}$ to the scales $|\mathbf{k}_h| > k_b$.

1. Introduction

Our understanding of the dynamics of strongly stratified flows has made an major step with the realization of the importance of the anisotropy and of the "buoyancy" scaling law which states that the vertical length scale of a structure should scale as the buoyancy length scale $L_b = U/N$, where U is the typical velocity of the structure and N is the Brunt-Väisälä frequency. This scaling law is valid in the inviscid limit as soon as the horizontal Froude number $F_h = U/(NL_h)$ (where L_h is the typical horizontal length scale) is small and implies that the potential energy is of the same order as the kinetic energy. Theoretically, it comes from the invariance of the Boussinesq Euler equations un-

† Present adress: Linné Flow Centre, KTH Mechanics, KTH, SE-100 44 Stockholm, Sweden
‡ Email address for correspondence: pierre.augier@mech.kth.se

der the hydrostatic approximation with respect to variation of the stratification (Billant & Chomaz 2001).

From the turbulence point of view, this scaling law leads to the hypothesis of a direct energy cascade (Lindborg 2002, 2006). Such cascade and the importance of the buoyancy length scale in strongly stratified turbulence has been observed in many numerical studies (Godeferd & Staquet 2003; Laval *et al.* 2003; Riley & de Bruyn Kops 2003; Waite & Bartello 2004; Lindborg 2006; Hebert & de Bruyn Kops 2006; Brethouwer *et al.* 2007; Lindborg & Brethouwer 2007).

As soon as the buoyancy Reynolds number $\mathcal{R} = ReF_h{}^2$ is very large (where Re is the usual Reynolds number, $Re = UL_h/\nu$, with ν the viscosity), it exists an universal regime of strongly stratified turbulence associated to a horizontal kinetic energy spectrum of the form $C_1 \varepsilon_K{}^{2/3} k_h^{-5/3}$, with $C_1 = 0.5$ an universal constant (Lindborg 2006; Brethouwer *et al.* 2007).

Actually, this $k_h^{-5/3}$ horizontal energy spectrum for strongly stratified turbulence is followed by a weakly stratified cascade at small scales (Brethouwer *et al.* 2007). The strongly stratified inertial range has been predicted to exhibit vertical spectra of the form $N^2 k_z^{-3}$. On the contrary, the weakly stratified cascade is nearly isotropic and thus associated to a $\varepsilon_K{}^{2/3} k_z^{-5/3}$ vertical spectrum. The transition between the two regimes happens at the Ozmidov length scale $l_o = \sqrt{\varepsilon_K/N^3}$, for which the horizontal Froude number $F_h(l_o) = u(l_o)/(Nl_o)$ is of order unity, where $u(l_o) = \varepsilon_K{}^{1/3} l_o^{-1/3}$ is the characteristic velocity associated to the length scale l_o.

However, numerous numerical simulations of stratified turbulence report mixing events due to the shear instability (Riley & de Bruyn Kops 2003; Laval *et al.* 2003; Hebert & de Bruyn Kops 2006; Brethouwer *et al.* 2007). As shown by Riley & de Bruyn Kops (2003), the inverse of the buoyancy Reynolds number is an estimate of the minimum value of the Richardson number that can be reached when vertical diffusion balances horizontal transport. Thus, the condition $\mathcal{R} > 1$ can be interpreted as a condition for the development of the shear instability in stratified turbulence. In addition, the Richardson number is related to the vertical Froude number $Ri \sim (NL_v/U)^2 \sim 1/F_v{}^2$ so that overturnings might develop already at vertical length scales L_v of the order of the buoyancy length scale L_b, i.e. at scales larger than the Ozmidov length scale l_o.

The evolution of a counter-rotating vortex pair in a stratified fluid has been extensively studied, in particular because it is one of the simplest flow on which the zigzag instability develops and from which the buoyancy length scale naturally emerges as the vertical length (Billant & Chomaz 2000*a*,*b*,*c*; Otheguy *et al.* 2006; Billant *et al.* 2010). Recently, Deloncle *et al.* (2008), Waite & Smolarkiewicz (2008) and Augier & Billant (2011) have investigated the nonlinear development of the zigzag instability. They have shown that both the shear and gravitational instabilities appear at high buoyancy Reynolds number when the zigzag instability has a finite amplitude leading to a transition to turbulence. This simple flow is interesting to unfold the nonlinear processes and instabilities since they occur successively in time whereas they all operate simultaneously in stratified turbulence.

In this paper, we continue the numerical study of the transition to turbulence in this particular case of a dipole. In contrast to previous studies, we focus on the spectral properties and transfers. In section 2, we describe the initial conditions and the numerical methods. The evolution of the spectra for a moderate horizontal Froude number is described in details in section 3. The effect of the horizontal Froude number is studied in section 4 and those of the Reynolds number in section 5. A spectral analysis of the

non-linear transfers is presented in section 6. Finally, conclusions are offered in the last section.

2. Methods

The methods are similar to those employed in Augier & Billant (2011). The numerical simulations are initialized by a Lamb-Chaplygin columnar dipole weakly perturbed by the dominant mode of the zigzag instability. The incompressible Navier-Stokes equations under the Boussinesq approximation are solved by means of a pseudo-spectral method with periodic boundary conditions (see Deloncle *et al.* (2008) for details).

The Reynolds number Re and the horizontal Froude number F_h are based on the initial conditions: $Re = UR/\nu, F_h = U/(NR)$, where U and R are respectively the velocity of translation and the radius of the Lamb-Chaplygin dipole and ν is the kinematic viscosity. The Schmidt number $Sc = \nu/\kappa$, where κ is the mass diffusivity, is set to unity in all runs. The Brunt-Väisälä frequency is given by $N = \sqrt{-(g/\rho_0)(d\bar{\rho}/dz)}$, where g is the gravity, ρ_0 a reference density, $\bar{\rho}(z)$ the basic density profile and z the vertical coordinate. The total density is given by $\rho_{tot} = \rho_0 + \bar{\rho}(z) + \rho'(x, y, z, t)$, where ρ' is the density perturbation and (x, y) the horizontal Cartesian coordinates. For simplicity and without loss of generality, R and R/U are taken respectively as length and time units. The density perturbations are non-dimensionalized by $Rd\bar{\rho}/dz$. The vertical length of the numerical box $\mathcal{L}_z$ is taken equal to the vertical wavelength of the dominant mode of the zigzag instability $\lambda_{zz}/R \simeq 10F_h$ (Billant & Chomaz 2000c). In the sequel, the buoyancy length scale will be set to this length scale $L_b = \lambda_{zz} = 10U/N$.

Most of the simulations are performed for the same Reynolds number: $Re = 28000$. In contrast, the Froude number is varied from $F_h = 0.0225$ (strong stratification) to $F_h = 0.135$ (moderate stratification). Thus a large range of buoyancy Reynolds number is covered going from 14 to 510, i.e. always well above the threshold for the shear and gravitational instabilities $\mathcal{R}_c \simeq 4.1$ for the Lamb-Chaplygin dipole (Augier & Billant 2011). The parameters of the runs are summarized in table 1.

In order to achieve such high Reynolds number, our methods differ from those employed in Augier & Billant (2011) in four main points: first, the horizontal size of the box is $\mathcal{L}_h = 4$ instead of $\mathcal{L}_h = 10$. We have verified that the development of the zigzag, shear and gravitational instabilities are weakly affected by this stronger lateral confinement due to the periodic boundary conditions. Only the late wake evolution differs when the pancake dipoles issued from the zigzag instability have then travelled more than the horizontal size of the box and the amplitude of the zigzag instability is larger than the box size. Then, the dipoles interact with their images due to the periodicity. Second, we use an adaptable time step procedure which maximizes the time step over a Courant-Friedrichs-Lewy condition (Lundbladh *et al.* 1999).

Third, in order to reduce the computational cost, the resolution in the x and y directions is increased during the run so as to adapt to the smallest scales of the flow. We start with a horizontal resolution $N_x \times N_y = 384 \times 384$. When the zigzag instability becomes nonlinear ($t = 3$), the resolution is increased to 768×768 and when the secondary instabilities develop ($t = 3.7$), it is set to 1024×1024. The runs for these 3 different resolutions are labelled S, M and L respectively (table 1). For each horizontal resolution, the number of numerical points over the vertical N_z is chosen so as to have a nearly isotropic mesh $N_z \simeq (\mathcal{L}_z/\mathcal{L}_h)N_x$. For $F_h = 0.09$, an additional simulation (labeled L2, see table 1) with an even higher resolution $1280 \times 1280 \times 320$ has been performed to check the convergence. Finally, to ensure the numerical stability, we have added to the classical dissipation an isotropic hyperviscosity $-\nu_4|\mathbf{k}|^8$, where $\mathbf{k}$ is the wavenumber and ν_4 a

Run	F_h	$\mathcal{R} = ReF_h{}^2$	${\mathcal{L}_h}^2 \times \mathcal{L}_z$	${N_h}^2 \times N_z$	ν_4	$\max_t \left(\frac{\varepsilon_{\nu_4}(t)}{\varepsilon(t)}\right)$	$\max_t(\varepsilon_K(t))$
Fh0.0225S	0.0225	14	$4^2 \times 0.225$	$384^2 \times 24$	1.8×10^{-18}	0.63	0.088
Fh0.0225M	0.0225	14	$4^2 \times 0.225$	$768^2 \times 48$	9.3×10^{-21}	0.40	0.082
Fh0.0225L	0.0225	14	$4^2 \times 0.225$	$1024^2 \times 64$	1.1×10^{-21}	0.31	0.082
Fh0.045S	0.045	57	$4^2 \times 0.45$	$384^2 \times 48$	1.8×10^{-18}	0.71	0.075
Fh0.045M	0.045	57	$4^2 \times 0.45$	$768^2 \times 96$	9.3×10^{-21}	0.50	0.088
Fh0.045L	0.045	57	$4^2 \times 0.45$	$1024^2 \times 128$	1.1×10^{-21}	0.38	0.087
Fh0.09S	0.09	227	$4^2 \times 0.9$	$384^2 \times 96$	1.8×10^{-18}	0.73	0.066
Fh0.09M	0.09	227	$4^2 \times 0.9$	$768^2 \times 192$	9.3×10^{-21}	0.49	0.070
Fh0.09L	0.09	227	$4^2 \times 0.9$	$1024^2 \times 256$	1.1×10^{-21}	0.36	0.069
Fh0.09L2	0.09	227	$4^2 \times 0.9$	$1280^2 \times 320$	1.7×10^{-22}	0.25	0.069
Fh0.135S	0.135	510	$4^2 \times 1.35$	$384^2 \times 144$	1.8×10^{-18}	0.73	0.063
Fh0.135M	0.135	510	$4^2 \times 1.35$	$768^2 \times 288$	9.3×10^{-21}	0.49	0.063
Fh0.135L	0.135	510	$4^2 \times 1.35$	$1024^2 \times 384$	1.1×10^{-21}	0.36	0.062

TABLE 1. Overview of the physical and numerical parameters of the simulations. For all simulations $Re = 28000$. The number of nodes in the x-, y- and z-direction are denoted, respectively, N_x, N_y and N_z. We recall that the length and time units is R and R/U respectively. $\varepsilon_{\nu_4}(t)$, $\varepsilon(t)$ and $\varepsilon_K(t)$ denote respectively the hyperviscous dissipation, the total dissipation and the dissipation of kinetic energy.

constant coefficient. From the lowest to the highest resolution, the value of the hyperviscosity ν_4 is decreased such as only the modes with the highest wavenumbers significantly contribute to the hyperviscous dissipation. For each resolution, the hyper-dissipation rate $\varepsilon_{\nu_4}(t)$ is observed to suddenly increase at a particular time when the highest wavenumber modes start to be filled. The resolution is increased before this time, i.e. before that the hyperviscosity affects the flow (except for the highest resolution).

The lack of resolution can be quantified by the temporal maxima (which is at the maximum of dissipation) of the ratio $\varepsilon_{\nu_4}(t)/\varepsilon(t)$, where $\varepsilon(t)$ is the total energy dissipation rate. This quantity would tend to 0 if the resolution were increased enough to perfectly resolve the Kolmogorov length scale. In table 1, the value of this parameter is reported for each run (note that all simulations are continued largely after the maximum of dissipation). It is around 0.3-0.4 for the largest simulations. A careful comparison of the run Fh0.09L and Fh0.09L2 corresponding to the same set of parameters but to two different resolutions does not show any differences in physical and spectral space apart from the width of the dissipative range. Indeed, the maximum of the ratio $\varepsilon_{\nu_4}(t)/\varepsilon(t)$ has decreased from 0.36 to 0.25. This indicates that, when the resolution is large enough, the non-dissipative part of the flow starts to be independent of the resolution and of the associated hyperviscosity suggesting that it would also be the same if a DNS were carried out. Because we do not seek to study the detailed structure of the dissipative range, such hyperviscosity allows us to decrease the width of the dissipation range and achieve higher Reynolds number values, i.e. increase the width of the inertial range for a given computational cost.

3. Global description of a simulation with $F_h = 0.09$

As already described by Deloncle *et al.* (2008), Waite & Smolarkiewicz (2008) and Augier & Billant (2011), the zigzag instability develops linearly at the beginning of the simulation and bends the dipole. By $t = 3.3$, the amplitude of the bending deformations

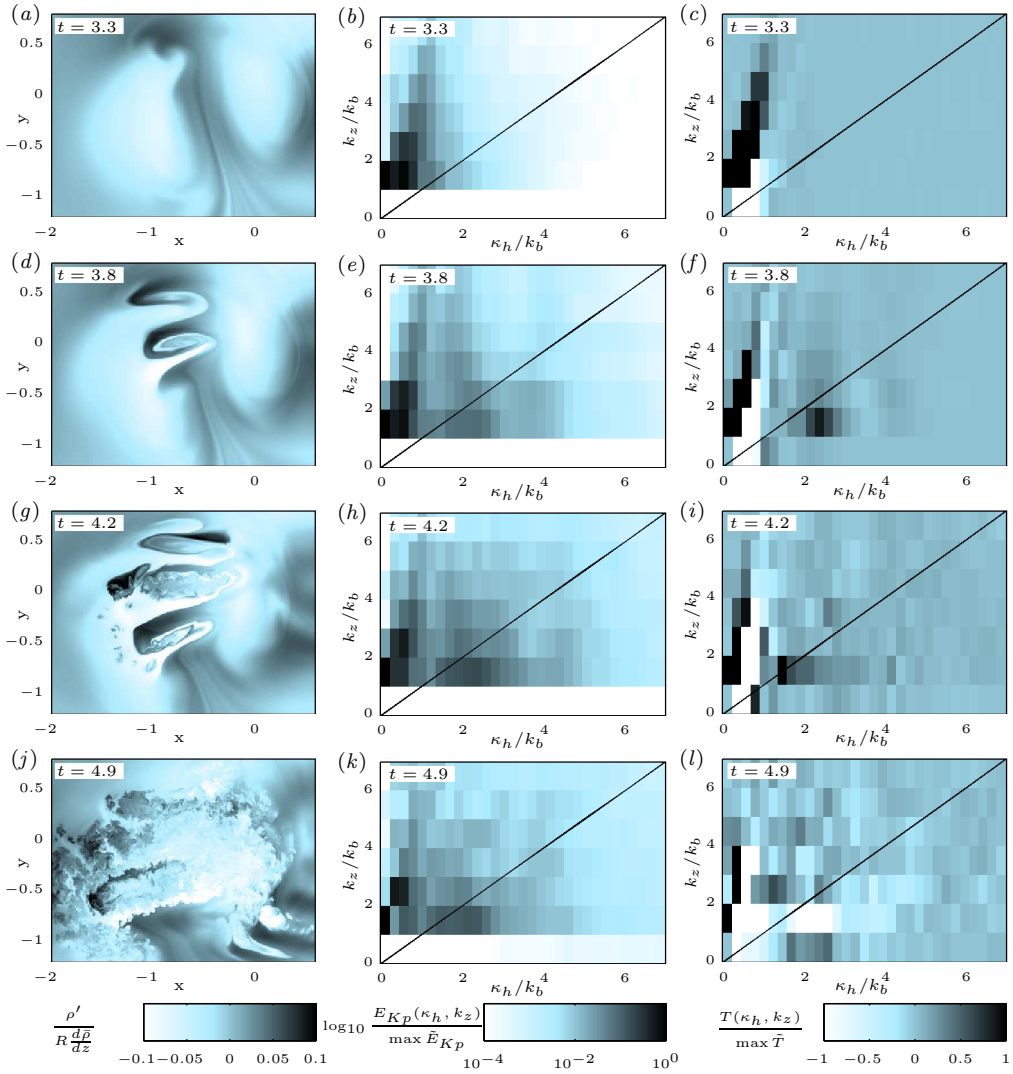

FIGURE 1. Description of four different characteristic times: $t = 3.3$ (a,b,c), $t = 3.8$ (d,e,f), $t = 4.2$ (g,h,i) and $t = 4.9$ (j,k,l) for $F_h = 0.09$. (a,d,g,j) show horizontal cross-sections of the density field at the level at which the shear instability begins to develop $z = 0.66\mathcal{L}_z$; (b,e,h,k) show the spectrum of poloidal energy $E_{Kp}(\kappa_h, k_z)$ and (c,f,i,l) display the total nonlinear energy transfer $T(\kappa_h, k_z)$.

is large but no secondary instability is yet active (Augier & Billant 2011). Thus, we begin our description of the flow at $t = 3.3$.

Figures $1(a,d,g,j)$ present the time evolution of the density field for $F_h = 0.09$ in a horizontal cross-section at the level at which the shear instability appears $z = 0.66\mathcal{L}_z$. At $t = 3.8$, small scale wiggles can be seen (Figure $1d$). They are associated to the roll up of Kelvin-Helmholtz (KH) billows with an horizontal axis as described by Deloncle *et al.* (2008) and Augier & Billant (2011). At time $t = 4.2$ (figure $1g$), the destabilization of the KH billows start to generate disordered small scales. Eventually, just after the maximum of dissipation, i.e. at $t = 4.9$, these small scales invade the whole domain (figure $1j$).

To analyze the properties of these small scales, we first use the poloidal-toroidal decomposition (Cambon 2001) also known as the Craya-Herring decomposition (Craya 1958;

Herring 1974) which expresses simply in Fourier space as $\hat{\mathbf{u}} = \hat{\mathbf{u}}_p + \hat{\mathbf{u}}_t$ for each wavenumber, where $\hat{\mathbf{u}}_p = -\boldsymbol{e_\theta} \times (\boldsymbol{e_\theta} \times \hat{\mathbf{u}})$ and $\hat{\mathbf{u}}_t = (\boldsymbol{e_\theta} \cdot \hat{\mathbf{u}})\boldsymbol{e_\theta}$ with $\hat{\mathbf{u}}$ the velocity in Fourier space, $\boldsymbol{e_\theta}$ the unit vector parallel to $\boldsymbol{e_z} \times \mathbf{k}$, where $\boldsymbol{e_z}$ is the vertical unit vector and $\mathbf{k}$ the wave vector. In the limit of small vertical Froude number, the poloidal velocity $\hat{\mathbf{u}}_p$ is associated to gravity wave and the toroidal velocity $\hat{\mathbf{u}}_t$ to potential vorticity modes. It has to be stressed that this interpretation is not legitimate here since the vertical Froude number reaches value order unity. The zigzag, KH and Rayleigh-Taylor instabilities induce an increase of the poloidal kinetic energy $\hat{E}_{Kp}(\mathbf{k}) = |\hat{\mathbf{u}}_p|^2/2$ and of the potential energy $\hat{E}_P(\mathbf{k}) = |\hat{\rho'}|^2/(2{F_h}^2)$ even if there is no waves (see e.g. Staquet & Riley 1989). Nevertheless, the toroidal-poloidal decomposition is used here only as a convenient formal decomposition enlightening the occurrence of vertical velocity without over interpreting its meaning in term of waves and vortices. Since the poloidal velocity does not correspond to vertical vorticity, its representation allows us to follow in Fourier space both the development of the non-linear zigzag instability with the strongly deformed dipole and the Kelvin-Helmholtz instability. From the energy in Fourier mode $\hat{E}_{Kp}(\mathbf{k})$, we define a two-dimensional poloidal energy spectral density

$$E_{Kp}(\kappa_h, k_z) = \frac{1}{\delta\kappa_h \delta k_z} \sum_{\mathbf{k} \in \delta\Omega_{[\kappa_h, \pm k_z]}} \hat{E}_{Kp}(\mathbf{k}), \tag{3.1}$$

where $\delta k_z = 2\pi/\mathcal{L}_z$, $\delta\kappa_h = 2\pi/\mathcal{L}_h$ and $\delta\Omega_{[\kappa_h, \pm k_z]}$ is a volume made of two rings ($k_z = \pm|k_z|$) defined by the relation ${\kappa_h}^2 \leqslant {k_x}^2 + {k_y}^2 < (\kappa_h + \delta\kappa_h)^2$.

Figures 1(*b,e,h,k*) show for the same instants as figures 1(*a,d,g,j*) the poloidal kinetic energy density $E_{Kp}(\kappa_h, k_z)$. Both vertical and horizontal wavenumbers are scaled by $k_b = 2\pi/L_b = 2\pi/\mathcal{L}_z$ which corresponds to the lowest non-zero vertical wavenumber and to the most amplified wavenumber of the zigzag instability. At $t = 3.3$, the poloidal kinetic energy is concentrated at $k_z = k_b$ and $\kappa_h \simeq 0\text{-}k_0$, where k_0 is the leading horizontal wavenumber of the 2D base flow. This feature is associated to the zigzag instability that has a finite amplitude. The energy is spread out at higher vertical wavenumbers than k_b as a result of the nonlinear development of the zigzag instability.

Figure 1(*c,f,i,l*) show the two-dimensional spectral density of total nonlinear energy transfers defined by the relation

$$T(\kappa_h, k_z) = \frac{1}{\delta\kappa_h \delta k_z} \sum_{\mathbf{k} \in \delta\Omega_{[\kappa_h, \pm k_z]}} \hat{T}(\mathbf{k}), \tag{3.2}$$

where $\hat{T}(\mathbf{k}) = -\Re[\hat{\mathbf{u}}^*(\mathbf{k}) \cdot (\widehat{\mathbf{u} \cdot \boldsymbol{\nabla}\mathbf{u}})(\mathbf{k}) + {F_h}^{-2} \hat{\rho'}^*(\mathbf{k})(\widehat{\mathbf{u} \cdot \boldsymbol{\nabla}\rho'})(\mathbf{k})]$, $\Re$ denoting the real part and the star the complex conjugate. The factor ${F_h}^{-2}$ in front of the second term comes from the non-dimensionalisation of the density perturbations (see section 2). In all the light regions, the transfer is negative meaning that these modes are loosing energy at the benefit of the wavenumbers in the dark regions. At $t = 3.3$ (figure 1*c*), the lost is maximum for the 2D mode $k_z = 0$, $\kappa_h = k_0$ and the gain is maximum at $k_z = k_b$, $\kappa_h \simeq 0\text{-}k_0$. This indicates that the zigzag instability is the leading mechanism extracting energy from the 2D base flow at that time. The black region extends vertically nearly up to $k_z \sim 6k_b$ and $\kappa_h \simeq k_b$. This confirms that the nonlinear development of the zigzag instability before the secondary instability is transferring energy to vertical harmonic modes of the initial preferred vertical wavenumber k_b corresponding to small vertical scales but not to horizontal scales smaller than the buoyancy length scale. Figure 1(*c*) also shows transfer toward the modes $k_z = k_b$ and $\kappa_h = 0$ which are the so-called "shear modes" reported by Smith & Waleffe (2002).

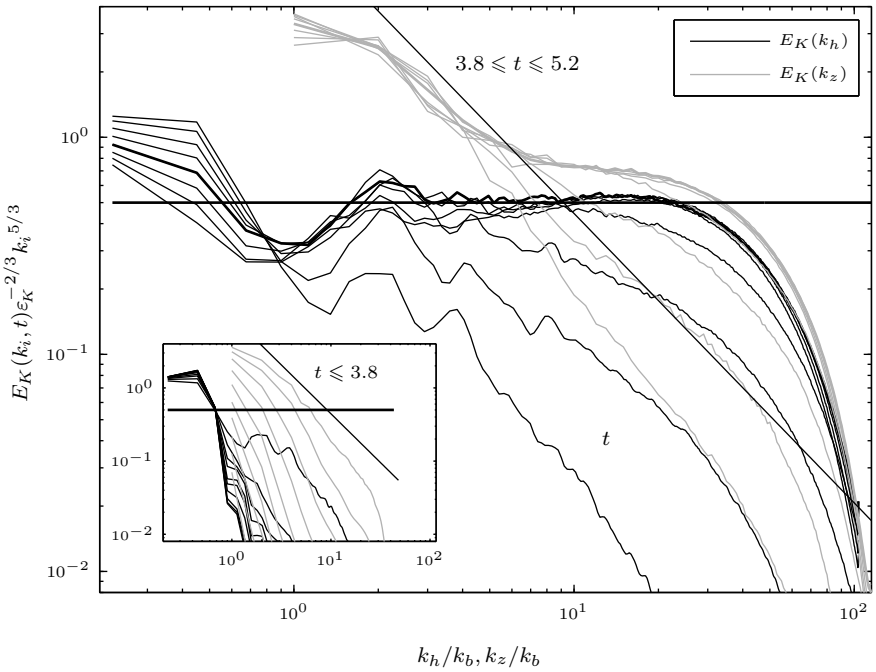

FIGURE 2. Time evolution of the horizontal and vertical compensated 1D spectra for $F_h = 0.09$ and $Re = 28000$. In the main plot, the spectra are shown for $t = 3.8$ to 5.2 with a time increment equal to 0.2. The inset plot shows the spectra for $t = 0.2$ to 3.8 with a time increment of 0.4. The thick curves correspond to the time for which the dissipation is maximum. The thin straight lines indicate the k_z^{-3} power law and the horizontal thick lines the $C\varepsilon_K^{2/3}k^{-5/3}$ law, with $C = 0.5$.

At $t = 3.8$, the energy transfer (figure 1f) exhibits a new peak close to $k_z \simeq k_b$ and $\kappa_h \simeq 2k_b$ (just below the diagonal isotropic line $\kappa_h = k_z$), due to the appearance of the KH instability which starts when the local Richardson number is small enough $Ri \lesssim 1/4$ (Deloncle *et al.* 2008). The wavenumber selected by the KH instability scales like the shear thickness which is proportional to the buoyancy length L_b when Ri is close to the critical value for instability. Therefore, the horizontal wavenumber selected by the secondary KH instability scales like k_b. Poloidal kinetic energy (figure 1e) presents then a secondary peak around $\kappa_h \simeq k_b$ just below the "isotropic" diagonal ($\kappa_h = k_z$). At $t = 4.2$, the appearance of small scales due to the destabilization of the KH billows (figure 1g), corresponds to positive transfers (figure 1i) toward high horizontal wavenumbers and a lost of energy at low horizontal wavenumbers. The poloidal kinetic energy spectrum exhibits a more isotropic shape with energy distributed nearly uniformly along the semi-circular lines ${k_z}^2 + {\kappa_h}^2 = const$ (figure 1h). At $t = 4.9$ (figure 1l), there are eventually transfers toward very small scales and all the scales corresponding to the earlier development of the KH billows are now loosing energy (bright region). It can be noticed that during all this process, the modes $k_z \simeq k_b$-$3k_b$ and $\kappa_h \simeq k_0$ are still gaining energy indicating that the primary zigzag instability remains active despite the development of the secondary shear and gravitational instabilities.

In figure 2, we have plotted several horizontal (black curves) and vertical (grey curves) instantaneous compensated unidimensional spectra $E_K(k_h)\varepsilon_K^{-2/3}{k_h}^{5/3}$ and $E_K(k_z)\varepsilon_K^{-2/3}{k_z}^{5/3}$, respectively, for the time $3.8 \leqslant t \leqslant 5.2$ corresponding to the development and the destabilization of the KH billows. The inset plot shows also the spectra for

$t \leqslant 3.8$, i.e. prior to the development of the shear instability. ε_K is the maximum kinetic energy dissipation rate and the horizontal unidimensional spectra are computed in the same way as in Lindborg (2006) as the mean value of the k_x and the k_y spectra,

$$E_K(k_h) = \frac{1}{2\delta k_h}\left[\sum_{\substack{|k_x|=k_h \\ k_y,k_z}} \hat{E}_K(\mathbf{k}) + \sum_{\substack{|k_y|=k_h \\ k_x,k_z}} \hat{E}_K(\mathbf{k})\right] \tag{3.3}$$

where $\delta k_h = 2\pi/\mathcal{L}_h$ and $\hat{E}_K(\mathbf{k}) = |\hat{\mathbf{u}}|^2/2$. Note the difference between the horizontal wavenumber k_h and κ_h the modulus of the horizontal wave vector. The thin straight lines indicate the k^{-3} power law and the horizontal thick lines display the $C\varepsilon_K^{2/3}k^{-5/3}$ law, with $C = 0.5$.

In the inset plot, we see that during the early evolution of the zigzag instability, the horizontal spectra does not vary. Only after $t > 3.2$, does the energy at horizontal wavenumbers larger than the buoyancy wavenumber k_b start increasing. In sharp contrast, the level of the vertical spectra increases nearly linearly in time in this logarithmic representation since the energy in the first mode grows exponentially owing to the development of the zigzag instability. For the penultimate time of the inset $t = 3.4$, the slope of the vertical spectra approaches k_z^{-3} even if only the zigzag instability has developed at that time. This indicates that this characteristic slope is mainly due to the vertical deformations of the dipole induced by the zigzag instability.

Starting at $t = 3.4$, we can see a peak in the horizontal spectra around $k_h/k_b = 2$ and its harmonics at $k_h/k_b = 4$ and 8. This is due to the appearance of the secondary KH instability. We observe a dip in the horizontal spectra between the small horizontal wavenumber k_0 corresponding to the initial dipole and $k_h/k_b = 2$. This is consistent with the observation of figure 1 where a direct transfer from the $[\kappa_h, k_z] \simeq [k_0, k_b]$ modes to the $[\kappa_h, k_z] \simeq [2k_b, k_b]$ modes due to the KH instability was evidenced. Beyond $t = 4.4$, energy eventually cascades toward the small horizontal scales with a slope close to $k_h^{-5/3}$ over approximately one decade. Remarkably, the horizontal spectra nearly perfectly collapse on the $C{\varepsilon_K}^{2/3}k_h^{-5/3}$, with $C = 0.5$, as observed in forced strongly stratified turbulence (Lindborg 2006; Brethouwer *et al.* 2007). However, the particular value of this constant is here not meaningful since it depends on the horizontal size of the computational domain compared to the dipole size. This is because the turbulence is concentrated around the vortices and is not homogeneous along the horizontal directions. Therefore, the observed agreement with the theory of strongly stratified turbulence is fortuitous. Quite remarkably, small vertical scales develop at the same time as the horizontal scales and, after $t = 4.4$, the vertical spectra exhibit a break in the slope around $k_z/k_b = 8$ where the slope goes from k_z^{-3} to $k_z^{-5/3}$. The $k_z^{-5/3}$ power law begins when the vertical spectrum k_z^{-3} approaches the horizontal one indicating a return to isotropy.

On figure 3, instantaneous toroidal (black), poloidal (light grey) and potential (dark grey), horizontal (figure 3*a*) and vertical (figure 3*b*) spectra are presented for $t = 4.6$ which correspond to the time where the dissipation is maximum. The large horizontal scales are dominated by the toroidal component while the peak at horizontal scales $\kappa_h = 2k_b$ is largely dominated by the poloidal and the potential components. At smaller horizontal scales, the toroidal and poloidal spectra approach each other. In figure 3(*b*), we see that the large vertical scales are also dominated by the toroidal spectra which confirms that the nearly k_z^{-3} slope in figure 2 is due to the non-linear vertical deformations of the dipole generated by the zigzag instability.

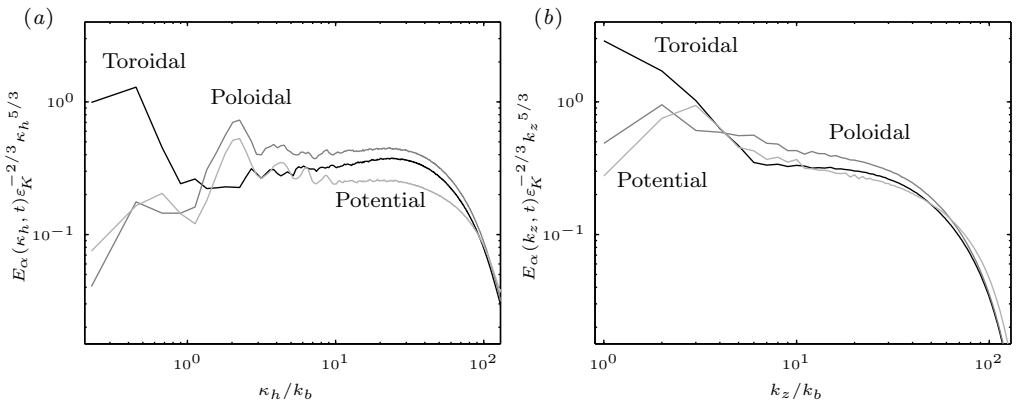

FIGURE 3. Horizontal (a) and vertical (b) compensated two-dimensional spectra of toroidal, poloidal and potential energy for $F_h = 0.09$ and $Re = 28000$ at $t = 4.6$. Black, dark grey and light grey curves correspond respectively to toroidal, poloidal and potential energies.

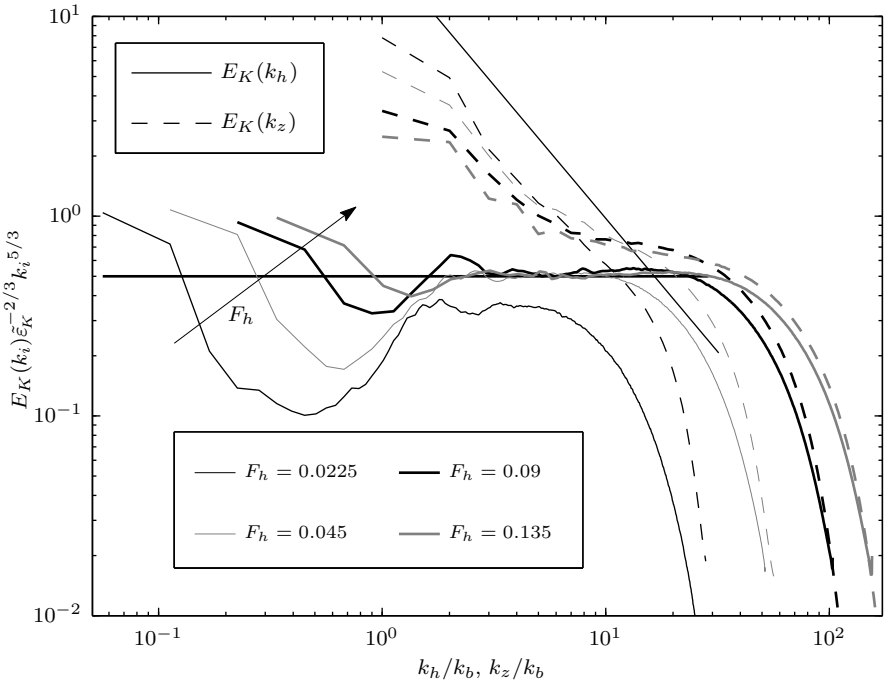

FIGURE 4. Horizontal and vertical compensated spectra $E_K(k_i)\tilde{\varepsilon}_K^{-2/3}k_i^{5/3}$ as a function of the dimensionless wavenumber k_i/k_b for four runs with different values of the Froude number $F_h = 0.0025$, 0.045, 0.09 and 0.135 but the same Reynolds number $Re = 28000$. Each curve is the average over time interval $\Delta t = 0.3$ near the maximum of the dissipation. The thin straight line indicates the k_z^{-3} power law and the horizontal thick line the $C\tilde{\varepsilon}_K{}^{2/3}k^{-5/3}$ law, with $C = 0.5$.

4. Variation of F_h and $\mathcal{R}$

Figure 4 presents horizontal (continuous curves) and vertical (dashed curves) compensated kinetic spectra $E_K(k_h)\tilde{\varepsilon}_K{}^{2/3}k_h{}^{5/3}$ and $E_K(k_z)\tilde{\varepsilon}_K{}^{2/3}k_z{}^{5/3}$ obtained from simulations with different values of F_h but the same Reynolds number $Re = 28000$. The spectra

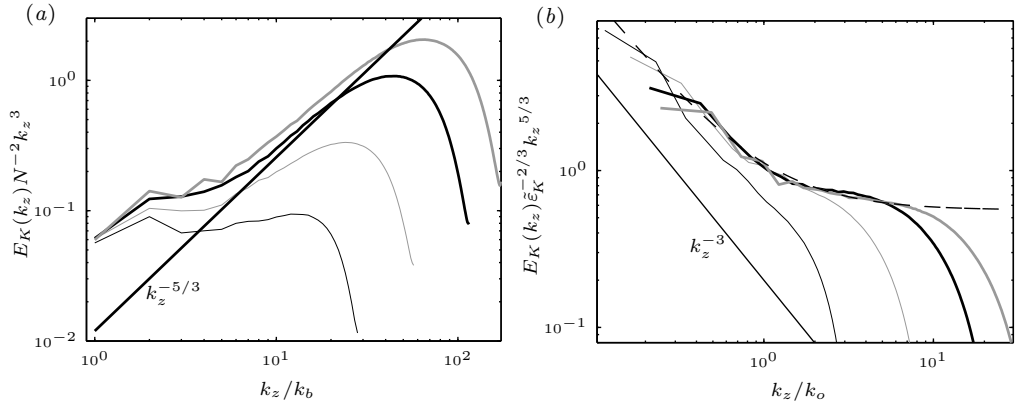

FIGURE 5. Vertical spectra already presented in figure 4 plotted in (a) as $E_K(k_z)N^{-2}{k_z}^3$ versus k_z/k_b and in (b) as $E_K(k_z)\tilde{\varepsilon}_K^{-2/3}{k_z}^{5/3}$ versus k_z/k_o. In (a), the thick straight line indicates the $k_z^{-5/3}$ power law. In (b), the thin straight line indicates the k_z^{-3} power law and the dashed line represents the theoretical expression (4.1).

have been time-averaged over $\Delta t = 0.3$ around the time where the total dissipation is maximum.

In order to rescale quantities, we use the maximum kinetic dissipation rate for $F_h = 0.09$: $\tilde{\varepsilon}_K = 0.069$. As seen in table 1, ε_K varies only weakly with F_h. This is because $\tilde{\varepsilon}_K$ can be considered as the energy injection rate which is independent of F_h since the initial state is identical for all simulations. In any case, the plot would have been very similar if each curve were scaled by its maximum dissipation rate ε_K.

All the vertical spectra begin at the same dimensionless wavenumber $k_z/k_b = 1$ because the vertical size of the numerical box is adjusted to the dominant wavelength of the zigzag instability. While Re is the same for all runs, the dissipative ranges extend to larger values of k_h/k_b when F_h is increased because k_b decreases. For the same reason, the horizontal spectra also move to the right when F_h increases since the lowest horizontal wavenumber is the same for all the simulations. For all the Froude numbers, the spectra are depleted in energy between the small horizontal wavenumbers and $k_h = k_b$. Remarkably, all the runs except for $F_h = 0.0225$ present for higher wavenumbers $k_h \gtrsim 2k_b$, a flat compensated horizontal spectra (corresponding to a $k_h^{-5/3}$ power law) collapsing at a value approximately equal to 0.5. For $F_h = 0.0225$ (black continuous thin line), the constant is lower probably because of the too low value of the buoyancy Reynolds number ($\mathcal{R} = 14$).

The vertical spectra are very steep near $k_z = k_b$ and show a tendency to follow a k_z^{-3} slope. They flatten when approaching the horizontal spectra at large wavenumber and their slope tends to $k_z^{-5/3}$ except for the highest stratification $F_h = 0.0025$, where the two curves approach each other only in the dissipation range (i.e. the Ozmidov scale is of the order of the Kolmogorov scale).

Figure 5(a) presents the same vertical spectra but now compensated by $N^2k_z^{-3}$, i.e. $E_K(k_z)N^{-2}{k_z}^3$. All the curves collapse to $E_K(k_z)N^{-2}{k_z}^3 = C_N \simeq 0.1$ for $k_z = k_b$ corresponding to the dominant mode of the zigzag instability. However, the curves depart rapidly from this constant when k_z increases all the more than F_h is large. This is because the transition to the $k_z^{-5/3}$ power law occurs at a lower vertical wavenumber when F_h increases.

Spectra scaling like $N^2k_z^{-3}$ are widely observed in nature (see e.g. Garrett & Munk

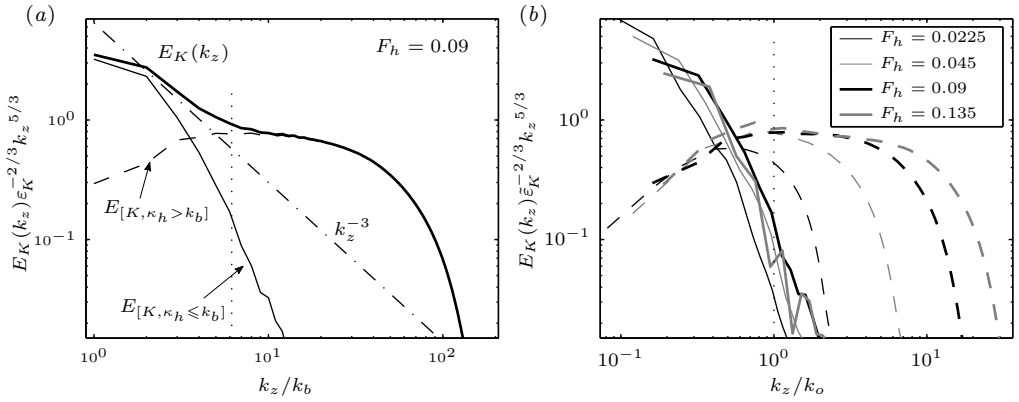

FIGURE 6. Decomposition of the vertical compensated spectra for $F_h = 0.09$ (a) and for all Froude numbers (b) shown in figure 4. In (a), the black thin curve corresponds to the vertical spectrum $E_{[K,\kappa_h\leqslant k_b]}(k_z)$ computed with modes for which $\kappa_h \leqslant k_b$ and the dashed curve to the spectrum $E_{[K,\kappa_h>k_b]}(k_z)$ computed with modes for which $\kappa_h > k_b$. The dotted lines indicate the Ozmidov wavenumber $k_z = k_o$. The dotted dashed lines show the k_z^{-3} power law. In (b), the solid curves correspond to the spectra $E_{[K,\kappa_h\leqslant k_b]}(k_z)$ and the dashed curves to the spectra $E_{[K,\kappa_h>k_b]}(k_z)$.

1979; Gregg 1987) and many authors (e.g. Lumley 1964; Holloway 1983; Dewan 1997; Brethouwer *et al.* 2007; Riley & Lindborg 2008) have predicted with dimensional analysis based on different theories that this spectrum should be followed by a $\varepsilon_K^{2/3}k_z^{-5/3}$ spectrum at small scales. We propose to express the total spectrum as the sum of a strongly stratified spectrum and an inertial spectrum, i.e. as

$$E_K(k_z) = C_N N^2 k_z^{-3} + C\varepsilon_K^{2/3}k_z^{-5/3} = ((k_z/k_o)^{-4/3}+1)C\varepsilon_K^{2/3}k_z^{-5/3} \qquad (4.1)$$

where C is a constant of order unity and $k_o = 2\pi/l_o$ with $l_o = 2\pi(C/C_N)^{3/4}(\varepsilon_K/N^3)^{1/2}$ the Ozmidov length scale. In figure 5(b), the compensated vertical spectra $E_K(k_z)\tilde{\varepsilon}_K^{-2/3}k_z{}^{5/3}$ are plotted as a function of k_z/k_o. Except for the Froude number $F_h = 0.0225$, all the curves collapse over a large range of vertical wavenumbers and in particular near the wavenumber of transition between the k_z^{-3} and the $k_z^{-5/3}$ power laws. This indicates that the change of slope occurs at the Ozmidov length scale as predicted for strongly stratified turbulence (Brethouwer *et al.* 2007). We can see that the spectrum (4.1) with $C_N = 0.08$ and $C = 0.56$ (dashed line) describes remarkably well the observed spectra except of course near the dissipative range. It has to be pointed out that the constant $C = 0.56$ associated to small scale turbulence is smaller than the classical Kolmogorov constant for homogeneous isotropic turbulence and unidimensional kinetic energy spectrum $C_K \simeq 1$ (Sreenivasan 1995; Monin & Yaglom 1975; Gotoh *et al.* 2002). However, the precise value of the constant C is here not meaningful and depends of the horizontal size of the numerical box because the turbulence does not invade all the computational domain.

Figure 6(a) presents a decomposition of the vertical compensated spectra $E_K(k_z)\varepsilon_K^{-2/3}k_z{}^{5/3}$ for $F_h = 0.09$. The continuous thin curve corresponds to conditional vertical spectrum $E_{[K,\kappa_h\leqslant k_b]}(k_z)$ computed with modes for which $\kappa_h \leqslant k_b$. As shown in figure 1, these modes correspond to the dipole deformed by the zigzag instability. This conditional vertical spectrum is very steep and clearly dominates the total spectrum at the largest vertical scales where the $N^2k_z^{-3}$ power law is observed. The dashed curve corresponds to conditional vertical spectrum $E_{[K,\kappa_h>k_b]}(k_z)$ computed with modes for

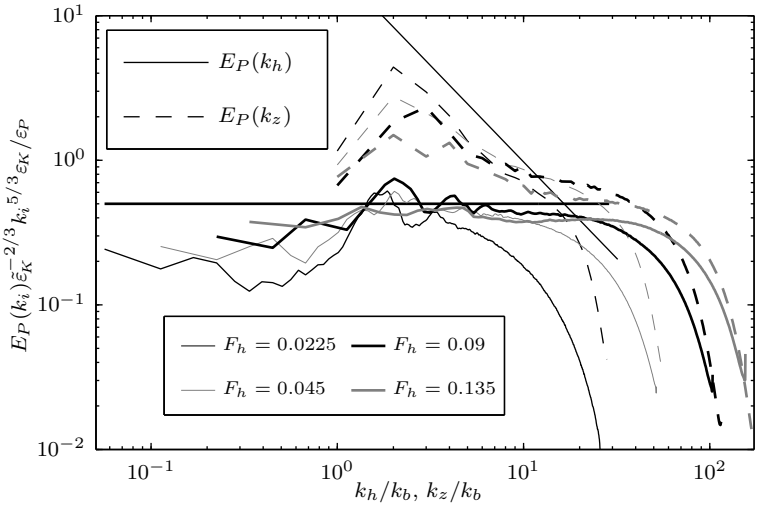

FIGURE 7. Similar to figure 4 except that it is the spectra of potential energy. The horizontal thick line shows the $0.5\tilde{\varepsilon_K}^{2/3}k^{-5/3}\varepsilon_P/\varepsilon_K$ law.

which $\kappa_h > k_b$. We have shown in figure 1 that these scales are generated mostly through the KH instability. We see that this conditional vertical spectrum is nearly flat from $k_z \simeq 3k_b$ to the dissipative range, i.e. the range corresponding to a $k_z^{-5/3}$ power law. This spectrum do not show any tendency to steepen at the largest vertical scales. This indicates that the turbulent structures generated through the shear instability are relatively isotropic with a $k^{-5/3}$ inertial range. This feature is hidden in the total vertical kinetic energy spectra at the large vertical scales between the buoyancy and the Ozmidov length scales owing to the dominance of the $N^2k_z^{-3}$ spectra associated to the large horizontal scales. The conditional spectra for the four Froude numbers are plotted in figure 6(b) as a function of k_z/k_o. This shows that the beginning of the $k_z^{-5/3}$ inertial range associated to small horizontal scales $\kappa_h > k_b$ scales with the Ozmidov wavenumber.

Figure 7 presents the horizontal (continuous lines) and vertical (dashed lines) compensated spectra $E_P(k_i)\tilde{\varepsilon_K}^{2/3}{k_i}^{5/3}\varepsilon_K/\varepsilon_P$ of potential energy for the four Froude numbers. An average over the same time interval has been performed as in figure 4. The potential spectra are very similar to the kinetic spectra (figure 4) but with less energy at large horizontal scales since the initial dipole has no potential energy. More pronounced bumps around the buoyancy length scale can be also seen. Like the horizontal compensated kinetic energy spectra $E_K(k_h)\tilde{\varepsilon_K}^{2/3}{k_h}^{5/3}$ (figure 4), the horizontal compensated potential energy spectra $E_P(k_h)\tilde{\varepsilon_K}^{2/3}{k_h}^{5/3}\varepsilon_K/\varepsilon_P$ present a flat range corresponding to a $k_h^{-5/3}$ power law from the buoyancy wavenumber to the dissipative wavenumber and nearly collapse at a value approximately equal to 0.5. This means that the relation $E_P(k_h)/\varepsilon_P = E_K(k_h)/\varepsilon_K$ approximatelly holds as observed in forced strongly stratified turbulence (Lindborg 2006; Brethouwer *et al.* 2007). However, the compensated spectra are slightly lower than predicted and slightly decrease over the inertial range before the dissipative range.

The total dissipation is plotted versus time on figure 8(a). For all Froude numbers, we see an increase at $t \simeq 3.7$ corresponding to the development of the KH instability. The dissipation before this time is mostly due to the vertical shear resulting from the development of the zigzag instability. It is thus approximately proportional to the inverse of the buoyancy Reynolds number. When the horizontal Froude number is increased, the dissipation peak tends to last a longer time, i.e. to be broader. This might be explained

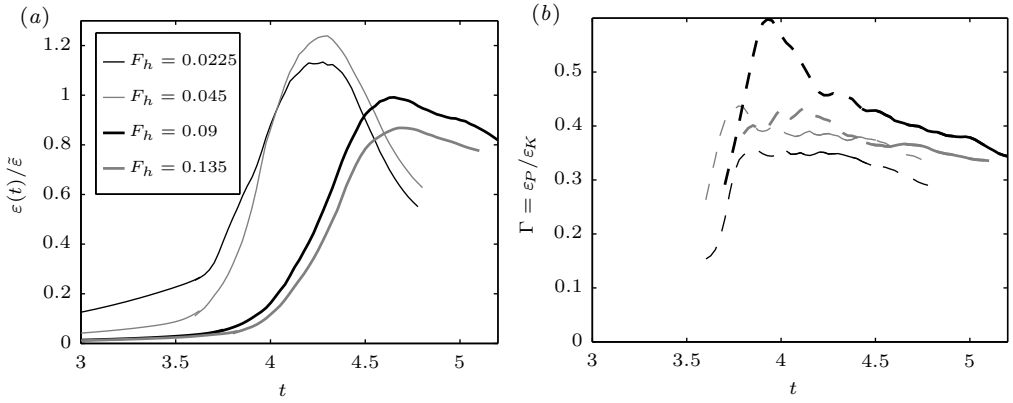

FIGURE 8. Temporal evolution of (a) the total dissipation rate $\varepsilon(t)$ for $F_h = 0.0025$, $F_h = 0.0045$, $F_h = 0.09$, $F_h = 0.135$ scaled by $\tilde{\varepsilon}$ the maximum dissipation rate for $F_h = 0.09$ and (a) the mixing efficiency $\Gamma = \varepsilon_P(t)/\varepsilon_K(t)$ (continuous lines are used when the dissipation rate is high $\varepsilon(t) > 0.8 \max \varepsilon(t)$).

by considering the properties of the KH billows as a function of F_h. We will show in section 5 that when the buoyancy Reynolds number is large enough, the shear instability is only weakly influenced by dissipation. Therefore, we shall neglect the dissipation even if this assumption is not valid for the smallest Froude number $F_h = 0.0225$ for which $\mathcal{R} = 14$. The vertical Froude number of the KH billows $F_{vKH} = \omega_h/(2N) \simeq (4Ri)^{-1/2}$, where ω_h is the dimensional horizontal vorticity, is of order unity for all F_h since $Ri \simeq 1/4$ at the onset of the shear instability. Since the dominant mode of the Kelvin-Helmholtz instability is characterized by a horizontal wavelength scaling like the shear thickness and a growth rate scaling like the shear (Hazel 1972), the shear instability transfers energy from the dipole with an horizontal scale R and characteristic time R/U toward small fast quasi-isotropic KH billows with characteristic length scale of order $U/N = F_h R$ and characteristic time of order $\omega_h^{-1} \sim N^{-1} = F_h R/U$. This may explain why the duration of the dissipation peak tends to decrease when the stratification increases.

Figure 8(b) presents the temporal evolution of the instantaneous mixing efficiency $\Gamma(t) \equiv \varepsilon_P(t)/\varepsilon_K(t)$. We see that the mixing efficiency is around 0.4 and weakly varies with the stratification and with the time period during which the dissipation is strong. We have also looked at the isotropy of the dissipation by considering the ratio $\varepsilon_z(t)/\varepsilon(t)$ where ε_z is the dissipation due to vertical gradients. The maximum value of $\varepsilon_z/\varepsilon$ increases with $\mathcal{R}$ and tends to $1/3$ which corresponds to an isotropic dissipation (not shown) even if a weak isotropic hyperviscosity is used.

5. Effects of the Reynolds number and of the resolution for $F_h = 0.09$

We now focus on the effects of the variation of the Reynolds number and of the resolution. Two additional simulations have been carried out for $F_h = 0.09$ and for the same resolution as for the simulation Fh0.09M, i.e. $N_h = N_x = N_y = 768$ and $N_z = 192$, but for different values of the Reynolds number $Re = 14000$ and $Re = 7000$. Figure 9(a) displays the horizontal compensated spectra $E_K(k_h)\tilde{\varepsilon}_K{}^{2/3}k_h{}^{5/3}$ for these two simulations with a lower Reynolds number and for the simulations Fh0.09M, Fh0.09L and Fh0.09L2 for which $Re = 28000$ (see table 1). We see that the width of the inertial range largely decreases when the Reynolds is decreased. However, the bump corresponding to the shear instability is nearly not affected meaning that, when the Reynolds number and

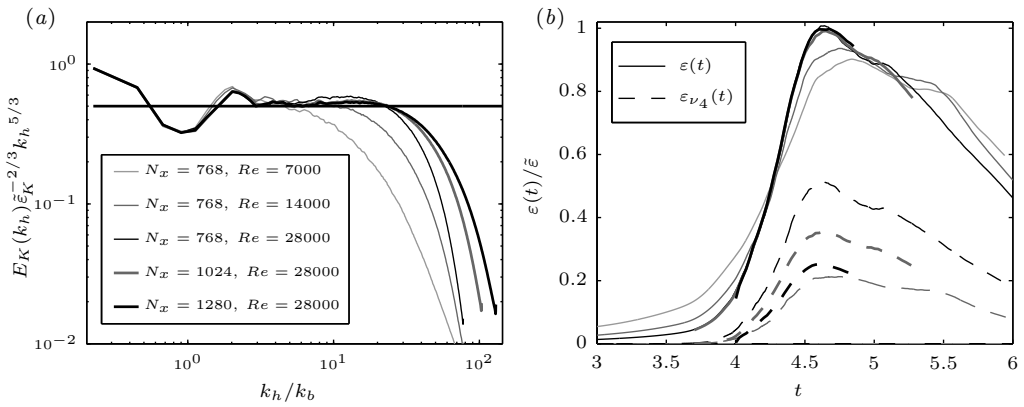

FIGURE 9. (a) Horizontal compensated spectra $E_K(k_h)\tilde{\varepsilon_K}^{2/3}{k_h}^{5/3}$ for five runs for different values of the Reynolds number and of resolution but for the same Froude number $F_h = 0.09$. Each curve is the average over time interval $\Delta t = 0.3$ near the maximum of the dissipation. The horizontal thick line shows the $0.5\tilde{\varepsilon_K}^{2/3}k_h^{-5/3}$ law. (b) Temporal evolution of the total dissipation rate $\varepsilon(t)$ (continuous lines) and of the hyper-dissipation rate $\varepsilon_{\nu_4}(t)$ (dashed lines) scaled by $\tilde{\varepsilon}$ the maximum dissipation rate for $Re = 28000$ and the maximum resolution $N_h = 1280$.

the buoyancy Reynolds number are large enough, the horizontal wavelength of the shear instability continues to scale with the buoyancy length scale. Besides, as already stated, there is nearly no differences between the two spectra for $N_h = 1024$ and $N_h = 1280$ apart at the smallest scales of the dissipative range, validating the use of a weak isotropic hyperviscosity.

The total dissipation (continuous lines) and the hyper-dissipation (dashed lines) are plotted versus time for the same runs on figure 9(b). We see that despite the important variation of resolution, the total dissipation curves for $Re = 28000$ (black thick and thin lines and grey thick line) are quite close, especially for the two largest simulations Fh0.09L and Fh0.09L2 (thick lines). In contrast, the hyper-dissipation strongly decreases when the resolution is increased indicating that the Kolmogorov scale becomes nearly resolved. For the lowest Reynolds number $Re = 7000$, there is no need for hyperviscosity and the simulation is a real DNS. The total dissipation curves for the different Reynolds numbers slightly differ. For lower Re, the dissipation is more important during the non-linear evolution of the zigzag instability before the development of the secondary instabilities occurring after $t = 3.7$. The increase corresponding to the development of the secondary instabilities is slightly slower leading to a slightly lower maximum of total dissipation of the order of $0.9\tilde{\varepsilon}$ for $Re = 7000$ and $0.94\tilde{\varepsilon}$ for $Re = 14000$. However, the global evolution of the total dissipation rate is only weakly affected by the variation of the Reynolds number. This indicates that the first mechanisms of the transition to turbulence, namely the non-linear evolution of the zigzag instability and the secondary instabilities, are only weakly influenced by dissipation for these values of buoyancy Reynolds number and of Reynolds number.

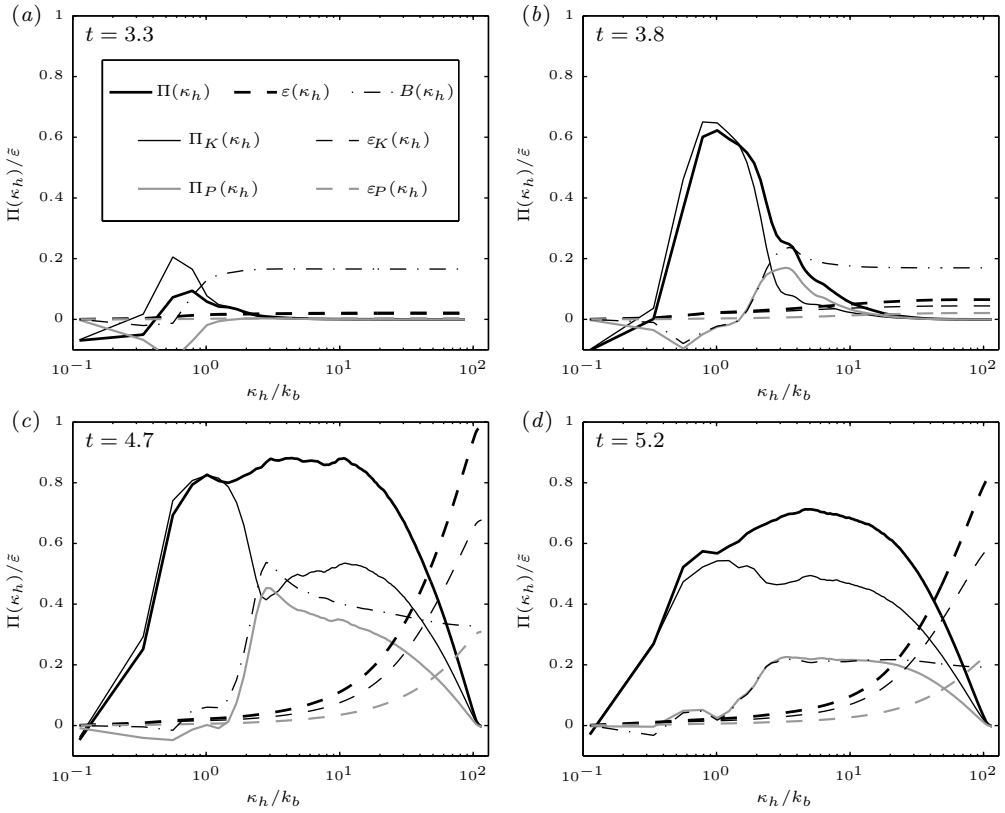

FIGURE 10. Fluxes going out from a vertical cylinder Ω_{κ_h} of radius κ_h in spectral space and dissipations inside this cylinder. The continuous black thin, grey and black thick curves are respectively the kinetic $\Pi_K(\kappa_h)$, potential $\Pi_P(\kappa_h)$ and total horizontal fluxes through the surface of Ω_{κ_h}. The dashed black thin, grey and black thick curves are respectively the kinetic $\varepsilon_K(\kappa_h)$, potential $\varepsilon_P(\kappa_h)$ and total dissipations inside the volume Ω_{κ_h}. The dotted dashed black curve is $B(\kappa_h)$ the sum inside the volume Ω_{κ_h} of $\hat{b}(\mathbf{k})$ the local conversion of kinetic energy into potential energy. The lowest wavenumber corresponds to the shear modes.

6. Decomposition of the horizontal fluxes for $F_h = 0.09$

The evolution equations of the kinetic and potential energies $\hat{E}_K(\mathbf{k}) = |\hat{\mathbf{u}}|^2/2$ and $\hat{E}_P(\mathbf{k}) = |\hat{\rho'}|^2/(2{F_h}^2)$ of a wavenumber $\mathbf{k}$ can be expressed as

$$\frac{d\hat{E}_K(\mathbf{k})}{dt} = \hat{T}_K - \hat{b} - \hat{D}_K, \tag{6.1}$$

$$\frac{d\hat{E}_P(\mathbf{k})}{dt} = \hat{T}_P + \hat{b} - \hat{D}_P, \tag{6.2}$$

where $\hat{T}_K = -\Re[\hat{\mathbf{u}}^*(\mathbf{k})\cdot(\widehat{\mathbf{u}\cdot\boldsymbol{\nabla}\mathbf{u}})(\mathbf{k})]$ and $\hat{T}_P = -F_h^{-2}\Re[\hat{\rho'}^*(\mathbf{k})(\widehat{\mathbf{u}\cdot\boldsymbol{\nabla}\rho'})(\mathbf{k})]$ are the kinetic and potential nonlinear transfers, $\hat{D}_K(\mathbf{k}) = |\mathbf{k}|^2|\hat{\mathbf{u}}|^2/Re$ and $\hat{D}_P(\mathbf{k}) = |\mathbf{k}|^2|\hat{\rho'}|^2/({F_h}^2 ReSc)$ are the kinetic and potential mean energy dissipation and $\hat{b}(\mathbf{k}) = F_h^{-2}\Re[\hat{\rho'}^*(\mathbf{k})\hat{w}(\mathbf{k})]$ is the conversion of kinetic energy into potential energy. When (6.1) and (6.2) are summed over the wavenumbers inside a vertical cylinder Ω_{κ_h} of radius κ_h in spectral space, we

obtain,

$$\frac{dE_K(\kappa_h)}{dt} = -\Pi_K(\kappa_h) - B(\kappa_h) - \varepsilon_K(\kappa_h), \tag{6.3}$$

$$\frac{dE_P(\kappa_h)}{dt} = -\Pi_P(\kappa_h) + B(\kappa_h) - \varepsilon_P(\kappa_h), \tag{6.4}$$

where $E_K(\kappa_h) = \sum_{|\mathbf{k}_h|\leqslant\kappa_h,k_z} \hat{E}_K(\mathbf{k})$, $\Pi_K(\kappa_h)$ is the kinetic flux going outside of Ω_{κ_h}, $B(\kappa_h)$ the conversion of kinetic energy into potential energy inside Ω_{κ_h} and $\varepsilon_K(\kappa_h)$ the kinetic dissipation inside Ω_{κ_h}. The quantities with the subscript P are defined similarly but for the potential energy. In order that the fluxes of the shear modes be not located at $-\infty$ in logarithmic plots, the horizontal wavenumber κ_h is discretized as $\kappa_h = \delta\kappa_h/2 + \delta\kappa_h l$, where $\delta\kappa_h = 2\pi/\mathcal{L}_h$ and l is the discretization integer.

These energy fluxes, conversion and dissipation rates are plotted versus κ_h for four particular times on figure 10 for $F_h = 0.09$ and $Re = 28000$. All the curves have been scaled by $\tilde{\varepsilon}$, the maximum of the total instantaneous dissipation. The plot for $t = 3.3$ (figure 10*a*) corresponds to a time where the zigzag instability evolves nonlinearly but the shear instability has not yet developed. At this time all the quantities are small compared to $\tilde{\varepsilon}$. The dissipation (dashed lines) is negligible. There is only a weak kinetic energy flux (black continuous line) of order $0.2\tilde{\varepsilon}$ toward horizontal wavenumbers slightly larger than the leading horizontal wavenumber of the 2D base flow k_0 (which is of order $0.4k_b$ for the particular stratification $F_h = 0.09$). By looking at the flux for other F_h, we have observed that the horizontal wavenumbers in which kinetic energy is transfered at this time do not scale as the buoyancy wavenumber but as k_0. The weakness of the transfer along the horizontal when only the zigzag instability is active is consistent with figure 1 which shows that the zigzag instability produces strong transfers along the vertical toward large vertical wavenumber of order k_b but only weak transfers along the horizontal. At wavenumbers slightly larger than k_0, $B(\kappa_h)$ increases from zero to approximately $0.17\tilde{\varepsilon}$ indicating a total conversion of kinetic into potential energies. Since $B(\kappa_h) = \sum_{|\mathbf{k}_h|\leqslant\kappa_h,k_z} \hat{b}(\mathbf{k})$, an increase (respectively decrease) of $B(\kappa_h)$ indicate positive (respectively negative) local conversion of kinetic into potential energies. The local conversion at wavenumber $\kappa_h \simeq k_0$ is due to the bending of the vortices. Remarkably, there is also a backward potential energy flux (grey continuous line) toward the smallest horizontal wavenumbers of the numerical box. However, the potential energy flux toward the horizontally invariant "shear modes" (located at the first point $\kappa_h \simeq 0.1k_b$ as explained previously) is zero. In contrast, kinetic energy flux is negative for the smallest wavenumber $\kappa_h \simeq 0.1k_b$, indicating a transfer of order $0.06\tilde{\varepsilon}$ to shear modes.

The time $t = 3.8$ (figure 10*b*) corresponds to the development of the KH billows before the transition to turbulence. As for $t = 3.3$, the dissipation (dashed lines) is negligible and there is a weak kinetic energy flux toward shear modes. The potential flux is still negative at large horizontal scales $0.1 \leqslant \kappa_h/k_b \lesssim 1$ and is now balanced by the energy conversion $B(\kappa_h)$. Kinetic energy flux becomes positive at $\kappa_h \simeq 0.3k_b$ (second point), reaches a maximum around $\kappa_h = 0.8k_b$ and drops down to nearly zero around $\kappa_h \simeq 3k_b$. This means that the kinetic energy is transferred from the large scales $\kappa_h \simeq k_0$ toward horizontal scales around $\kappa_h = 2k_b$. This transfer appears as a peak and not as a plateau because the ratio $2k_b/k_0$ is not large but only moderate for $F_h = 0.09$. However, the other runs for lower F_h (not plotted) show that this non-local transfer appears as a plateau with a width $2k_b/k_0$ proportional to F_h^{-1}. The conversion of kinetic into potential energies (grey dashed dotted curve) becomes positive at horizontal wavenumber $\kappa_h \simeq 1.5k_b$, reaches its maximum at $\kappa_h \simeq$ 3-4k_b and then slightly decreases and remains constant around 0.2ε

for smaller scales. Again, the increase of $B(\kappa_h)$ at k_b is due to the development of the KH billows which convert kinetic energy into potential energy at the buoyancy length scale. The slight decrease of $B(\kappa_h)$ at smaller scales corresponds to a weak conversion of potential energy back into kinetic energy.

Figure 10(c) corresponds to the time $t = 4.7$ when the dissipation is maximum. The total dissipation $\varepsilon(\kappa_h)$ (black thick dashed line) reaches the value $\tilde{\varepsilon}$ for the largest κ_h. The potential dissipation is approximately one third of the total dissipation. The kinetic energy flux at large scales is similar to the one for $t = 3.8$ with even a stronger flux from large scales toward $\kappa_h \simeq 2k_b$. The peak at large scales corresponding to the development of the KH billows has reached a value close to unity just before at $t = 4.5$. The conversion of kinetic into potential energies at wavenumbers $\kappa_h \simeq 2k_b$ is now much stronger indicating that the KH billows are efficient to displace isopycnals. At the wavenumber $\kappa_h \simeq 3k_b$, kinetic and potential fluxes are nearly equal. In contrast to figure 10(a), the total flux, equal to $0.8\tilde{\varepsilon}$ between k_0 and $2k_b$, does not drop to zero but reach another plateau close to $\Pi(\kappa_h)/\varepsilon = 0.9$ down to the dissipation range. This second plateau at small scales is different and due to the destabilization of the KH billows and to the gravitational instability. At small scales, there is a conversion of potential energy back into kinetic energy (the dotted dashed curve goes down) which is driven by these instabilities and the associated transition to turbulence. This conversion leads to an increase of the kinetic energy flux and a decrease of potential energy flux (grey continuous curve) with a nearly constant total energy flux. Besides, the upscale energy fluxes at large scales have significantly decreased.

At later time $t = 5.2$ (figure 10c), dissipation is still close to $0.8\tilde{\varepsilon}$ but the plateau of kinetic energy flux has decreased to $0.5\tilde{\varepsilon}$. The new feature is that the total transfer at small scales is now dominated by the kinetic energy flux, the potential energy flux being nearly 2 times smaller. This may be the sign of a restratification with weaker overturning events. Moreover, the potential flux is remarkably flat from $\kappa_h \simeq 3k_b$ to the dissipative range and there is no energy conversion. This may indicate that the density at small scales is passively advected during the late decay.

Since the initial flow has no potential energy and since the energy conversion at large scales is weak during the life time of the dipole, no potential energy is available at large scales and the cascade of potential energy toward small scales should exist at the expense of the kinetic energy. This is evidenced by the fact that potential energy transfer $\Pi_P(\kappa_h)$ is almost always equal to the conversion of kinetic energy into potential energy $B(\kappa_h)$. Remarkably, $B(\kappa_h)$ always becomes positive when $\kappa_h \gtrsim k_b$, i.e. for the scales created by the development of secondary instabilities.

7. Summary and conclusions

We have presented a spectral analysis of the transition to turbulence from a columnar dipole in a stratified fluid. A series of instabilities and non-linear processes occurs in a particular time sequence leading to a breakdown into small-scale turbulence.

We have shown that the transition to turbulence occurring during the nonlinear evolution of the zigzag instability has a two-step dynamics. First, a shear instability feeds quasi-isotropic and fast Kelvin-Helmholtz billows with a vertical Froude number of order unity and a typical scale of the order of the buoyancy scale, i.e. larger that the Ozmidov length scale. Second, the destabilisation of these structures and the gravitational instability generate a turbulence from the buoyancy scale to the dissipative range. This turbulent regime is weakly stratified because the associated larger structures are linked to vertical Froude number of order unity and are roughly isotropic, with horizontal and vertical

characteristic length scales of the same order. Moreover, significant vertical motions due to overturnings exist in this regime.

The spectra have been shown to be strongly anisotropic. The horizontal spectra exhibit a $k_h^{-5/3}$ inertial range. Nevertheless, there is a deficit of energy in the range between the large scales associated to the dipole and the buoyancy length scale. Remarkably, at smaller scales and down to the dissipative scales, the kinetic and potential energy horizontal spectra approximatively collapse respectively on the $0.5{\varepsilon_K}^{2/3}k_h^{-5/3}$ and $0.5{\varepsilon_K}^{2/3}k_h^{-5/3}\varepsilon_P/\varepsilon_K$ spectra. Thus the relation $E_P(k_h)/\varepsilon_P = E_K(k_h)/\varepsilon_K$ approximately holds as measured in numerical simulations of forced stratified turbulence. The vertical kinetic spectrum follows at large vertical scales a $C_N N^2 k_z^{-3}$ law, with $C_N \simeq 0.08$, which is due to the non-linear evolution of the zigzag instability. For the largest values of the buoyancy Reynolds number $\mathcal{R}$, the vertical spectrum presents a transition at the Ozmidov length scale l_o toward a $C{\varepsilon_K}^{2/3}k^{-5/3}$ spectrum, with $C \simeq 0.56$.

Thus, the anisotropic spectra share many characteristics with those obtained from numerical simulations of forced stratified turbulence and from measurements in the atmosphere and in the ocean. This is unexpected because the initial flow is very simple and not turbulent. Moreover, the fundamental difference between a transition toward turbulence and developed turbulence has to be stressed. With only two vortices interacting, the dynamics at large horizontal scales is dominated by the zigzag instability and there is no strongly stratified cascade along the horizontal. This contrasts with numerical simulations of forced stratified turbulence which exhibit a forward strongly stratified cascade but for which the overturning motions at the buoyancy length scale and beyond are not resolved or only weakly resolved due to the use of strongly anisotropic numerical meshes (see e.g. Koshyk & Hamilton 2001; Lindborg 2006; Waite 2011).

Since the transition in the vertical spectra happens at the Ozmidov length scale, it is tempting to conclude that the overturning motions at the buoyancy scale are strongly anisotropic. However, this is not the case. Indeed, we have shown that the very steep vertical spectrum is mainly due to the large horizontal scales of the dipole strongly deformed along the vertical by the zigzag instability. In contrast, the vertical spectrum computed with spectral modes with horizontal wavenumbers larger than the buoyancy wavenumber k_b does not present any k_z^{-3} power law but exhibits a $k_z^{-5/3}$ power law from a vertical wavenumber scaling like the Ozmidov wavenumber k_o down to the dissipative range.

In this paper, we have stressed the qualitative difference between the buoyancy length scale L_b and the Ozmidov length scale l_o. However, quantitatively, the ratio L_b/l_o scales like $F_h^{-1/2}$ and is therefore not very large for $F_h = O(0.1)$. In the present case, the Ozmidov wavenumber can be computed as

$$k_o = \left(\frac{C_N}{C}\right)^{3/4}\left(\frac{N^3}{\varepsilon_K}\right)^{1/2} = F_h^{-3/2}\left(\frac{C_N}{C}\right)^{3/4}\left(\frac{U^3}{\varepsilon_K R}\right)^{1/2}\frac{1}{R}, \tag{7.1}$$

and the buoyancy wavenumber $k_b = 2\pi/(10F_h)$. The ratio is therefore

$$\frac{k_o}{k_b} = F_h^{-1/2}\left(\frac{C_N}{C}\right)^{3/4}\left(\frac{U^3}{\varepsilon_K R}\right)^{1/2}\frac{10}{2\pi} \simeq 1.4F_h^{-1/2}, \tag{7.2}$$

and varies only from 9.3 to 3.8 when F_h increases from 0.0225 to 0.135.

It has to be pointed out that recent results highlight the importance of the buoyancy length scale on forced stratified turbulence (Waite 2011). Finally, we can conjecture that such nonlocal transfers due to secondary instabilities act as a leak from the strongly stratified turbulent cascade toward a weakly stratified turbulence beyond the buoyancy

scale. However, the horizontal scales larger than the buoyancy length scale dominate the vertical spectra down to the Ozmidov length scale.

REFERENCES

Augier, P. & Billant, P. 2011 Onset of secondary instabilities on the zigzag instability in stratified fluids. *J. Fluid Mech.* **662**, 120–131.

Billant, P. & Chomaz, J.-M. 2000*a* Experimental evidence for a new instability of a vertical columnar vortex pair in a strongly stratified fluid. *J. Fluid Mech.* **418**, 167–188.

Billant, P. & Chomaz, J.-M. 2000*b* Theoretical analysis of the zigzag instability of a vertical columnar vortex pair in a strongly stratified fluid. *J. Fluid Mech.* **419**, 29–63.

Billant, P. & Chomaz, J.-M. 2000*c* Three-dimensional stability of a vertical columnar vortex pair in a stratified fluid. *J. Fluid Mech.* **419**, 65–91.

Billant, P. & Chomaz, J.-M. 2001 Self-similarity of strongly stratified inviscid flows. *Phys. Fluids* **13**, 1645–1651.

Billant, P., Deloncle, A., Chomaz, J.-M. & Otheguy, P. 2010 Zigzag instability of vortex pairs in stratified and rotating fluids. part 2. analytical and numerical analyses. *J. Fluid Mech.* **660**, 396–429.

Brethouwer, G., Billant, P., Lindborg, E. & Chomaz, J.-M. 2007 Scaling analysis and simulation of strongly stratified turbulent flows. *J. Fluid Mech.* **585**, 343–368.

Cambon, C. 2001 Turbulence and vortex structures in rotating and stratified flows. *Eur. J. Mech. B - Fluids* **20**, 489–510.

Craya, A. D. 1958 Contribution à l'analyse de la turbulence associée à des vitesses moyennes. *Ministre de l'air, France* **PST 345**.

Deloncle, A., Billant, P. & Chomaz, J.-M. 2008 Nonlinear evolution of the zigzag instability in stratified fluids: a shortcut on the route to dissipation. *J. Fluid Mech.* **599**, 229–238.

Dewan, E. 1997 Saturated-cascade similitude theory of gravity wave spectra. *J. Geophys. Res.-Atmos.* **102** (D25), 29799–29817.

Garrett, C. & Munk, W. 1979 Internal waves in the ocean. *Annu. Rev. Fluid Mech.* **11**, 339–369.

Godeferd, F. S. & Staquet, C. 2003 Statistical modelling and direct numerical simulations of decaying stably stratified turbulence. Part 2. Large-scale and small-scale anisotropy. *J. Fluid Mech.* **486**, 115–159.

Gotoh, T., Fukayama, D. & Nakano, T. 2002 Velocity field statistics in homogeneous steady turbulence obtained using a high-resolution direct numerical simulation. *Phys. Fluids* **14** (3), 1065–1081.

Gregg, M. C. 1987 Diapycnal mixing in the thermocline - a review. *J. Geophys. Res.-Oceans* **92** (C5), 5249–5286.

Hazel, P. 1972 Numerical studies of the stability of inviscid stratified shear flows. *J. Fluid Mech.* **51**, 39–61.

Hebert, D. A. & de Bruyn Kops, S. M. 2006 Predicting turbulence in flows with strong stable stratification. *Phys. Fluids* **18**.

Herring, J. R. 1974 Approach of axisymmetric turbulence to isotropy. *Phys. Fluids* **17**, 859–872.

Holloway, G. 1983 A conjecture relating oceanic internal waves and small-scale processes. *Atm. Ocean* **21** (1), 107 – 122.

Koshyk, J. N. & Hamilton, K. 2001 The horizontal kinetic energy spectrum and spectral budget simulated by a high-resolution troposphere-stratosphere-mesosphere GCM. *J. Atmos. Sci.* **58** (4), 329–348.

Laval, J. P., McWilliams, J. C. & Dubrulle, B. 2003 Forced stratified turbulence: Successive transitions with Reynolds number. *Phys. Rev. E* **68** (3, Part 2).

Lindborg, E. 2002 Strongly stratified turbulence: a special type of motion. In *Advances in Turbulence IX, Proceedings of the Ninth European Turbulence Conference*. Southampton.

Lindborg, E. 2006 The energy cascade in a strongly stratified fluid. *J. Fluid Mech.* **550**, 207–242.

Lindborg, E. & Brethouwer, G. 2007 Stratified turbulence forced in rotational and divergent modes. *J. Fluid Mech.* **586**, 83–108.

Lumley, J. L. 1964 The spectrum of nearly inertial turbulence in a stably stratified fluid. *J. Atmos. Sci.* **21** (1), 99–102.

Lundbladh, A., Berlin, S., Skote, M., Hildings, C., Choi, J., Kim, J. & Henningson, D. S. 1999 An efficient spectral method for simulation of incompressible flow over a flat plate. *Trita-mek. Tech. Rep.* **11**.

Monin, A.S. & Yaglom, A.M. 1975 *Statistical Fluid Mechanics, vol. 2*. Cambridge MA, MIT Press.

Otheguy, P., Chomaz, J.-M. & Billant, P. 2006 Elliptic and zigzag instabilities on co-rotating vertical vortices in a stratified fluid. *J. Fluid Mech.* **553**, 253–272.

Riley, J. J. & de Bruyn Kops, S. M. 2003 Dynamics of turbulence strongly influenced by buoyancy. *Phys. Fluids* **15** (7), 2047–2059.

Riley, J. J. & Lindborg, E. 2008 Stratified Turbulence: A Possible Interpretation of Some Geophysical Turbulence Measurements. *J. Atmos. Sci.* **65**, 2416–2424.

Smith, L. M. & Waleffe, F. 2002 Generation of slow large scales in forced rotating stratified turbulence. *J. Fluid Mech.* **451**, 145–168.

Sreenivasan, K. R. 1995 On the universality of the Kolmogorov constant. *Phys. Fluids* **7** (11), 2778–2784.

Staquet, C. & Riley, J. J. 1989 On the velocity field associated with potential vorticity. *Dynamics of Atmospheres and Oceans* **14**, 93–123.

Waite, M. L. 2011 Stratified turbulence at the buoyancy scale. *Physics of Fluids* **23** (6), 066602.

Waite, M. L. & Bartello, P. 2004 Stratified turbulence dominated by vortical motion. *J. Fluid Mech.* **517**, 281–308.

Waite, M. L. & Smolarkiewicz, P. K. 2008 Instability and breakdown of a vertical vortex pair in a strongly stratified fluid. *J. Fluid Mech.* **606**.